JOURNAL OF AIRCRAFT
Vol. 38, No. 2, March–April 2001

Flight Test of Active Structural Acoustic Noise Control System

Dan Palumbo,* Ran Cabell,† and Brenda Sullivan†
NASA Langley Research Center, Hampton, Virginia 23681
and
John Cline‡
U.S. Army Research Laboratory, Hampton, Virginia, 23681

A flight test is described in which an active structural/acoustic control system reduces turboprop induced interior noise on a Raytheon Aircraft Company 1900D airliner. Control inputs to 21 inertial force actuators were computed adaptively using a principal component domain version of the multichannel filtered-x least mean square algorithm to minimize the mean square response of 32 microphones. A tabu search algorithm was employed to optimize placement of the force actuators on the aircraft frame. Both single-frequency and multifrequency control results are presented. Noise reductions of up to 15 dB were obtained at the blade passage frequency (BPF) during single-frequency control tests. Simultaneous noise reductions of 10 dB, 2.5 dB, and 3.0 dB, at the BPF and next 2 harmonics, were obtained in a multifrequency test.

Introduction

THE active structural acoustic control (ASAC) approach for noise control in aircraft cabins has been in development for several years.[1–5] ASAC differs from active noise control (ANC)[6,7] approach in actuation method; ANC uses loudspeakers vs ASAC's structural actuators.[8] The ASAC approach has been pursued with the expectation that a mature design would be more cost effective than an ANC system of comparable performance. Efficiency improvements are expected in installation costs, channel count, and channel power requirements.

Two technologies were tested in the ASAC design. First, the filtered-x least mean square (LMS)[9] controller was implemented in the principal component domain.[10] This provides processing efficiencies and controller stability beyond that of conventional controllers. Second, the actuator locations were optimized using a tabu search algorithm that was directed by predictions of noise reduction and control force.[11] Proper positioning of ASAC actuators has been shown to be critical in achieving good noise control while using minimal force.[11]

The flight test objectives were to demonstrate stable noise control of the first three harmonics of the blade passage frequency (BPF), verifying controller performance and validating the optimization predictions. Both single-frequency and multifrequency control were accomplished. The following sections present a description of the principal component controller, the optimization procedure, and the test configuration. Test results are then presented and discussed and concluding remarks are offered.

Principal Component Controller

The principal component least mean squares (PC-LMS) algorithm was used as the adaptive control algorithm. This algorithm is a transform domain version of the multichannel filtered-x LMS algorithm[9,12] and is described in detail elsewhere.[10] In PC-LMS, the controller parameters, that is, the filter weights, are adapted in a transformed coordinate system that decouples the multiple-input/multiple-output control channels at a single frequency. Each control channel in this transformed coordinate system is independent of every other channel. In contrast, the filter weights for the filtered-x algorithm are adapted in a coordinate system defined by the control actuators, which are not usually independent of one another and can show high degrees of interchannel coupling when many actuators are used. By decoupling the control channels, convergence rates and control effort penalties can be set for each channel independently.

A block diagram of a feedforward controller based on the multiple-error LMS algorithm is shown in Fig. 1. The response of the error sensors is given by the $(m \times 1)$ vector $\boldsymbol{e}$ and at a frequency ω as described by the expression

$$\boldsymbol{e}(\omega) = \boldsymbol{H}(\omega)\boldsymbol{w}(\omega) + \boldsymbol{d}(\omega) \tag{1}$$

The $(r \times 1)$ vector $\boldsymbol{w}$ represents the control inputs to the actuators, and the $(m \times r)$ matrix $\boldsymbol{H}$ contains transfer functions from the input of each actuator to the output of each error sensor at the frequency ω. The $(m \times 1)$ vector $\boldsymbol{d}$ contains the error sensor responses to the primary noise field and is called the primary response. The matrix $\hat{\boldsymbol{H}}(z)$ is an estimate of the physical error path transfer function matrix $\boldsymbol{H}(z)$ and is used to filter the reference signal.[7]

Each term in Eq. (1) depends on frequency ω, and this dependence is understood implicitly in subsequent equations. The frequency domain representation in Eq. (1) describes the controller operating at steady state, with no transients, and should not be used to analyze the effect of delays in the error path transfer functions on the controller.[12] The PC-LMS algorithm is obtained by substituting the singular value decomposition (SVD) of $\boldsymbol{H}$ into Eq. (1). The SVD of $\boldsymbol{H}$ is written

$$\boldsymbol{H} = \boldsymbol{U}\boldsymbol{S}\boldsymbol{V}^H \tag{2}$$

where superscript H denotes the complex conjugate transpose. The $(m \times m)$ matrix $\boldsymbol{U}$ and $(r \times r)$ matrix $\boldsymbol{V}$ contain the eigenvectors of $\boldsymbol{H}\boldsymbol{H}^H$ and $\boldsymbol{H}^H\boldsymbol{H}$, respectively. The $(m \times r)$ matrix $\boldsymbol{S}$ contains the square roots of the eigenvalues of $\boldsymbol{H}^H\boldsymbol{H}$. The singular values are decreasing, such that $s_1 > s_2 > \cdots > s_r$, where s_i is the ith singular value.

Substituting the SVD of $\boldsymbol{H}$ into Eq. (1) yields

$$\boldsymbol{e} = \boldsymbol{U}\boldsymbol{S}\boldsymbol{V}^H\boldsymbol{w} + \boldsymbol{d} \tag{3}$$

$$\boldsymbol{U}^H\boldsymbol{e} = \boldsymbol{S}\boldsymbol{V}^H\boldsymbol{w} + \boldsymbol{U}^H\boldsymbol{d} \tag{4}$$

$$\boldsymbol{\zeta} = \boldsymbol{S}\boldsymbol{\nu} + \boldsymbol{p} \tag{5}$$

The vector $\boldsymbol{\zeta} = \boldsymbol{U}^H\boldsymbol{e}$ represents the sensor responses mapped onto the principal components (PCs) of the control system, whereas

Received 10 November 1999; revision received 15 September 2000; accepted for publication 15 September 2000.

*Senior Aerospace Engineer, Structural Acoustics Branch. Member AIAA.
†Aerospace Engineer, Structural Acoustics Branch.
‡Aerospace Engineer, Structural Mechanics Division.

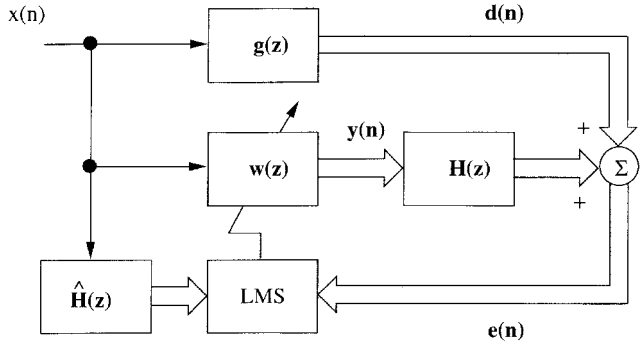

Fig. 1 Multiple-error LMS algorithm.

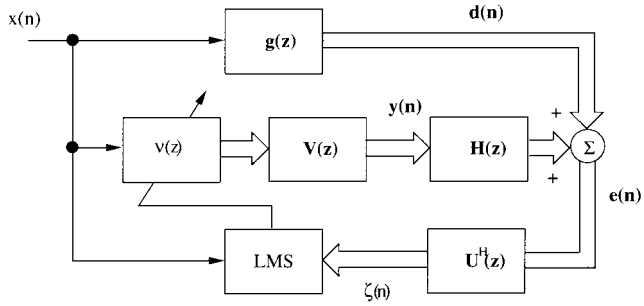

Fig. 2 Principal component LMS.

$\boldsymbol{\nu} = \boldsymbol{V}^H \boldsymbol{w}$ is the mapping of the actuator inputs onto the PCs. The vector $\boldsymbol{p} = \boldsymbol{U}^H \boldsymbol{d}$ is the mapping of the primary field onto the PCs. The columns of the matrix $\boldsymbol{U}$, therefore, constitute linear transformations from sensor responses to PCs, and the columns of $\boldsymbol{V}$ transform actuator inputs to PCs.[10,12] Expanding Eq. (5) term by term produces

$$\zeta_i = \begin{cases} s_i \nu_i + p_i & \text{for} \quad i = 1, \ldots, r \\ p_i & \text{for} \quad i = r+1, \ldots, m \end{cases} \tag{6}$$

assuming there are more error sensors than control actuators. Each PC error term ζ_i depends only on the corresponding PC control input ν_i and the mapping of the primary response onto the ith PC p_i. The last $(r+1)$ through m PCs are not controllable and constitute the residual field after control is applied.

Figure 2 contains a schematic of feedforward control implemented using the PC-LMS algorithm. The filter weights $\boldsymbol{\nu}$ are adapted in terms of the PCs of the controller, and then transformed using $\boldsymbol{V}$ into actuator coordinates. The sensor responses are likewise transformed into PC coordinates using $\boldsymbol{U}^H$ and are used in the recursive updates of the filter weights in PC coordinates. A recursive update for the PC control inputs ν_i can be derived from the update expression used in the multiple-error LMS algorithm. The resulting adaptive algorithm for the ith PC weight ν_i is written[10]

$$\nu_i(n+1) = \nu_i(n) - \mu_i s_i \zeta_i(n) \tag{7}$$

Combining the scalar step size μ_i and singular value s_i into a single scalar yields a generalized update

$$\nu_i(n+1) = \nu_i(n) - \alpha_i \zeta_i(n) \tag{8}$$

where α_i is the step size parameter for the ith principal component.

It is often necessary to constrain the control outputs so that they do not exceed physical limitations of the control actuators. There are two methods for constraining actuator inputs when the PC-LMS algorithm is used: 1) Set the step sizes α_i of the last few PCs to zero.[10] These PCs require the highest control effort. 2) Apply a control effort penalty or leak factor in the weight update recursion for some PCs. The update recursion with a control effort penalty is written

$$\nu_i(n+1) = [1 - (u_i/s_i)\beta_i]\nu_i(n) - \alpha_i \zeta_i(n) \tag{9}$$

The noise reduction potential of candidate control systems is calculated during actuator location optimization. For a feedforward control system, predictions of noise reduction and control effort require knowledge of the transfer function matrix $\boldsymbol{H}$, the primary response $\boldsymbol{d}$, and an estimate of the coherence between the reference and the primary response γ^2. The portion of the primary response at the ith microphone that is coherent with the reference signal and, therefore, controllable is written

$$d_i^{\text{coh}} = d_i \gamma_i \tag{10}$$

where γ_i is the coherence between the reference and the response of the ith microphone. When the PC transformation is applied to the coherent portion of the primary response, d_i^{coh} produces a vector of coherent PC responses, denoted p_i^{coh}. The predicted value of the control input to the ith PC is given by[10]

$$\nu_i^{\text{coh}} = \frac{-s_i p_i^{\text{coh}}}{s_i^2 + \beta_i} \tag{11}$$

The predicted control inputs in terms of actuator coordinates can be computed from the PC control inputs $\boldsymbol{\nu}^{\text{coh}}$ as

$$\boldsymbol{w} = \boldsymbol{V}\boldsymbol{\nu}^{\text{coh}} \tag{12}$$

These control input values can be substituted into Eq. (1) to obtain the residual error. Noise reduction, in decibels, can then be computed by

$$\Delta_{\text{dB}} = 10 \log_{10}(\boldsymbol{e}^H \boldsymbol{e} / \boldsymbol{d}^H \boldsymbol{d}) \tag{13}$$

Test Configuration

The test aircraft, a Raytheon 1990D, is shown in Fig. 3. The aircraft can carry 19 passengers 2900 km at a maximum cruise speed of 533 km/h. The aircraft cabin is 10.8 m long, 1.8 m high, and 1.4 m wide. The 1900D has a four-bladed propeller and associated BPF of ~103 Hz. The twin engines are phase locked through a synchrophaser at the shaft speed of 25.8 revolutions per second (rps). The test aircraft was untrimmed.

A list of the flight test equipment is given in Table 1, and a block diagram of the system is shown in Fig. 4. The control system used 32 microphones and 21 actuators. The controller, conditioners, amplifiers, and digital tape recorder were arranged in two racks.

Table 1 Equipment list

Item	Number
Controller	
Rack-mount PC	1
DSP board	1
I/O board	3; 48 in; 24 out
Tachometer interface	1
Acquisition	
ICP conditioners	3; 48 channels
Microphones	32
Accelerometers	12
Tape recorder	48 channels
Control	
Amplifiers	4; 24 channels
Actuators	21 pairs
Miscellaneous	
Oscilloscope	1
Monitor	1
Keyboard	1
Mouse	1

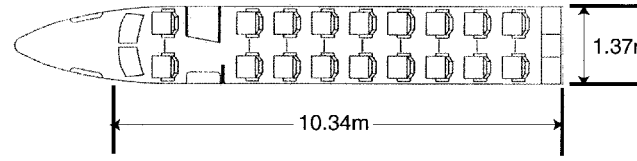

Fig. 3 Raytheon/Beech 1900 Cabin.

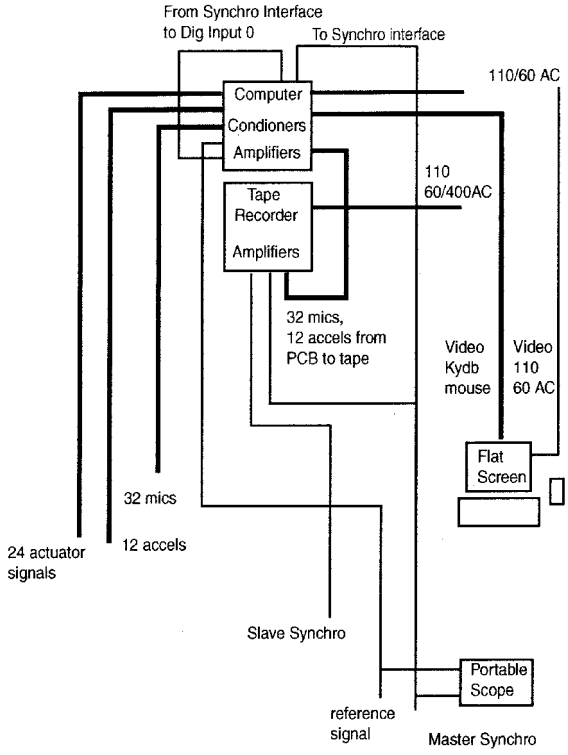

Fig. 4 System block diagram.

Controller

The controller consisted of a rack-mounted computer with digital signal processor (DSP), I/O, and tachometer interface. The DSP board contained two TMS320C40 processors, which were connected to three I/O boards. Each I/O board had 16 input and 8 output channels. A once-per-revolution pulse was obtained from the propeller shaft tachometer signal and used to trigger an interrupt on the DSP board. A phase lock loop tracked this interrupt signal and was used to generate a data sampling pulse at a frequency 48 times the once-per-revolution signal. With a nominal propeller shaft rate of 25.8 rps, the sampling rate for the control system was approximately 1238 Hz. Filters onboard the I/O boards were set to 723 Hz and provided–18-dB rolloff per octave.

Acquisition

The primary response was sampled with 0.25-in. electret condenser microphones with 30-mV/Pa sensitivity. The microphones were uniformly distributed, four microphones on a ring frame (as shown in Fig. 5) with the lower and upper microphones roughly corresponding to seated and standing head heights, respectively. In an effort to reduce near-field effects, the microphones were attached so that they protruded about 20 cm from the side wall. Eight frames in the passenger compartment of the aircraft were instrumented for a total of 32 microphones.

Actuation

The inertial actuators, type IFX 15, were made especially for installation on an aircraft ring frame (see Fig. 6). The actuators are designed to be mounted in pairs on the frame. Specifications for the actuator are summarized in Table 2. There were 21 actuator pairs installed for the flight test. The actuator resonant frequency (95 Hz) was tuned to be just below the 1900D BPF (103 Hz) to avoid the high rate of change of phase that typically occurs around resonance. The coil resistance (7.5 Ω) was chosen to be compatible with the multichannel audio amplifiers that were used to power the actuators.

Actuator Location Optimization

The actuator locations were selected through a process of combinatorial search with a goal to reduce interior noise and control effort. The tabu search method, with its straightforward approach and success record,[11] was chosen to optimize the actuator locations for the flight test.

A combinatorial search procedure such as tabu search combs through a large set of candidate actuator locations and selects a subset of a given size that best meets some goal or performance criteria. For the purpose of optimizing actuator locations for best noise reduction, a database of actuator acoustic response at each candidate location must be constructed, and a procedure for predicting

Table 2 Specifications for IFX 15 actuators

Parameter	Value
Peak force	75 N (17 lbf) at 103 Hz
Power	12 W
Resistance	7.5 Ω (dc)
Resonant frequency	95 Hz
Weight	245 g (0.5 lb)
Dimensions	64 × 25 × 36 mm (2.5 × 1 × 1.4 in.)

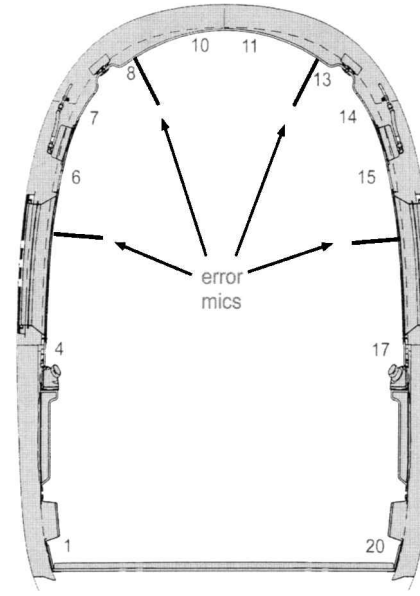

Fig. 5 Frame bay and microphone locations.

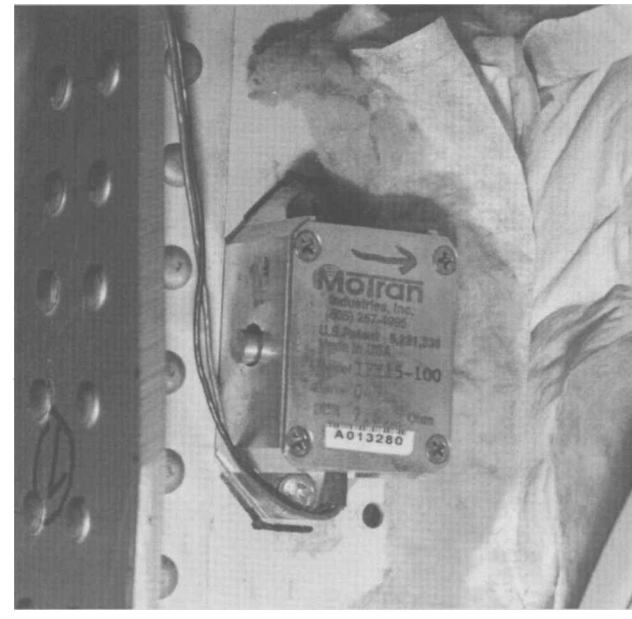

Fig. 6 Inertial actuator mounted to 1900D frame.

the noise reduction for any subset of actuator responses must be established.

The effectiveness of the tabu search algorithm hinges on the accuracy of the cost function (predicted noise reduction) and the coverage of the candidate set. An absolutely accurate cost function is not necessary for optimization. However, a good prediction is useful for making tradeoff studies of the number of actuators needed to meet a specific noise reduction goal. Acquiring the data necessary to construct the candidate set is challenging because it requires obtaining a representative sample of the actuator response at all of the possible locations. A method of predicting the noise reduction that incorporates coherence and constraints is given in Eqs. (11–13). The next section will describe how the actuator location candidate set was obtained.

Actuator Location Survey

To optimize the actuator locations at a given frequency, a matrix of transfer functions between the input to an actuator at each candidate location and the microphone outputs must be assembled. Analytical methods are not yet capable of modeling the structural/acoustic response of an airframe with the fidelity needed to create this matrix, and so an experimental approach was employed. This approach involved placing an actuator at each candidate location, driving it with a tone at the frequency of interest, and computing the transfer function to each microphone response. To avoid the time consuming process of drilling holes and bolting the actuator at each location, it was proposed that the actuator be clamped to the frame temporarily. The use of a single clamped actuator had the drawback that the relationship between the clamped actuator response and a bolted actuator-pair response was unknown. A preliminary test was performed that validated the use of the clamped actuator for the survey. The actuator/clamp assembly was able to be fitted to 82 locations on the 1900D frame. There were 32 microphones mounted as described in the section on test configuration. Transfer functions were obtained at the BPF and four higher harmonics.

Pressurization Effects

The actuator location survey was done on the ground in an unpressurized cabin. Pressurizing the cabin could alter the structural/acoustic actuator transfer functions and, thus, affect the performance of the PC domain controller.[10] If these changes were significant, they could invalidate the results of the actuator location optimization. An evaluation of the pressurization effects was made using a finite element model of an aluminum cylinder complete with ring frames and stringers. The interior acoustics were modeled with a boundary element model. The results of these simulations, summarized in Table 3, demonstrate that pressurization changes similar to those experienced at cruise altitude can have a significant effect on the performance and stability of an ASAC system.[13] Table 3 shows noise control predictions for unpressurized and pressurized operating conditions. Both conditions use transfer functions obtained in unpressurized conditions. Note that no noise reduction is obtained under pressurized conditions at the higher harmonics. Based on these results, it can be expected that the actuator set optimized with ground-based transfer functions will not perform as predicted, especially in the higher harmonics. At the very least, the transfer function data should be measured in flight, before the noise control experiment, to restore lost performance. However, selection of truly optimal actuator locations may require in-flight measurement of transfer functions for all candidate actuator locations.

Table 3 Effect of cabin pressurization on predicted noise control

	ΔdB				
Condition	104 Hz	208 Hz	312 Hz	416 Hz	520 Hz
Unpressurized	−17.9	−2.6	−1.8	−3.6	−4.1
Pressurized	−13.1	——	——	——	——

Multifrequency Optimization

Multifrequency actuator location optimization was accomplished using total noise reduction over the frequencies of interest as the search cost function. This cost function is written as

$$J_{\text{tot}} = \sum_{i=1}^{n} a_i^2 J_i \tag{14}$$

where the parameters a_i are defined according to the weighting method being used. Three weighting methods were evaluated: linear, decibel-A, and loudness level. Loudness level weighting indicated there would be no subjective benefit from controlling the higher harmonics. Linear and A weighting showed similar effects, that is, the fourth and fifth harmonic may not be worth controlling, and very little benefit is gained from the second and third. For these reasons the optimization was performed using the linear sum of the squared pressures of the first three harmonics to calculate the total noise reduction.

PC Optimization

One of the features of the PC controller is that increased stability and performance can be achieved by not controlling the higher principal components that are associated with smaller singular values and higher control forces. This functionality can be simulated by using the PC domain noise prediction equations as given by Eqs. (10–13) as the optimization cost function.

As an example, consider a 12-actuator, 32-microphone control system. Selecting a random set of actuators from the database of 82 possible locations results in values for the principal components of the primary field p_i as shown in Fig. 7. This system will not achieve good noise reduction because too much acoustic power is concentrated in the higher-order elements of p_i, for example, the 18th which are either uncontrollable or difficult to control (due to small singular values). A set of actuators optimized using force constraints improves the design by shifting more acoustic power into the 12 controllable PCs (Fig. 8). Here, the majority of the acoustic power is concentrated into the first few PCs, matching the authority available in the larger singular values. A force constrained optimization is obtained by incorporating force constraints into the noise control solution (see Ref. 14 for details). This can be done in either of two ways, calculating a unique constraint matrix for each solution (using, for example, a constraint minimization algorithm) or estimating a single conservative constraint matrix that satisfies all solutions (as in Ref. 15). The former produces a more accurate noise reduction prediction, but places additional computational burden on the optimization algorithm. The latter method has little overhead and, although not accurate, produces results that are adequate for optimization purposes.

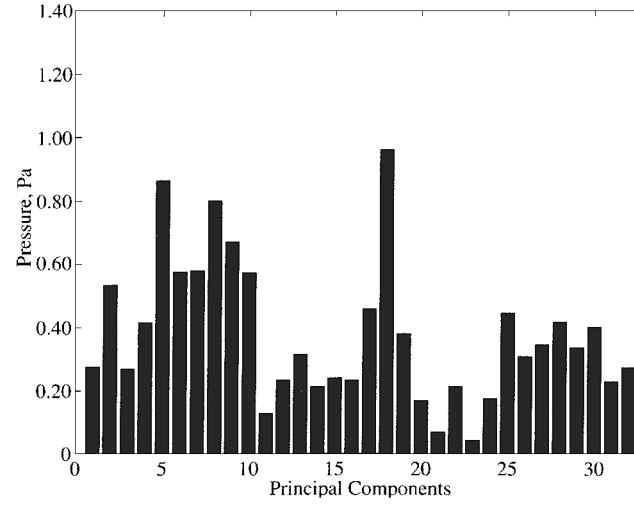

Fig. 7 PCs using a random actuator set.

Table 4 Predicted noise control for optimized actuator configuration

	ΔdB			
Weighting	Overall	BPF	2BPF	3BPF
Linear	−12.9	−13.5	−8.6	−6.3
A weighted	−10.8	−13.5	−8.7	−6.4

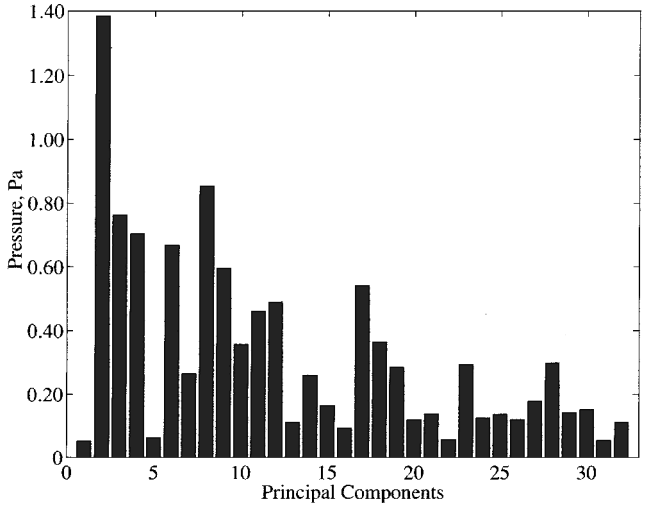

Fig. 8 PCs using optimized actuators.

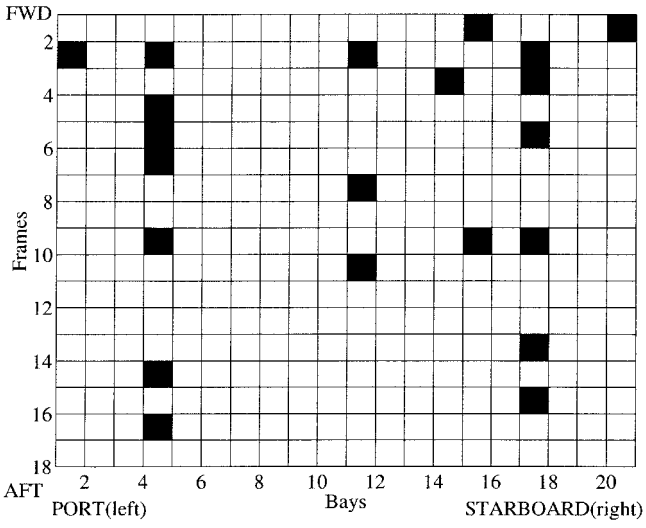

Fig. 9 Actuator mounting locations on 1900D.

Optimization Results

The actuator set used in the noise control flight tests were selected using a force constrained optimization (see section "PC Optimization") over the first three harmonics. Figure 5 shows the numbering for some of the bays on the 1900D frame. Figure 9 shows all 21 actuator locations in a view where the frames are unwrapped, bay 1 on the port or left side. The first frame is closest to the cockpit, just behind the door, and is placed at the top of Fig. 9.

The predicted noise reduction is listed in Table 4 for linear and A-weighted cases. Although the A weighting produces a smaller overall noise reduction figure, the value of the first harmonic (BPF) reduction is identical to the linear case, and the values of the second and third harmonics (2BPF and 3BPF, respectively) increase only slightly. This is further evidence of the dominance of the first harmonic.

The noise controller used only the first 18 principal components due to processing limitations, and so it was important to concentrate

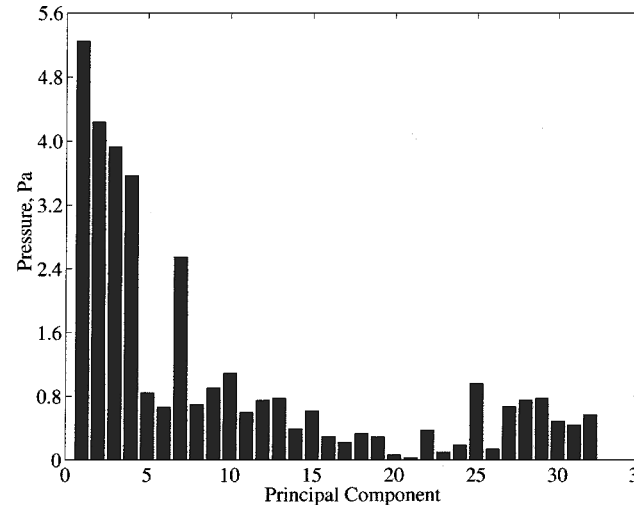

Fig. 10 Primary PCs, first harmonic.

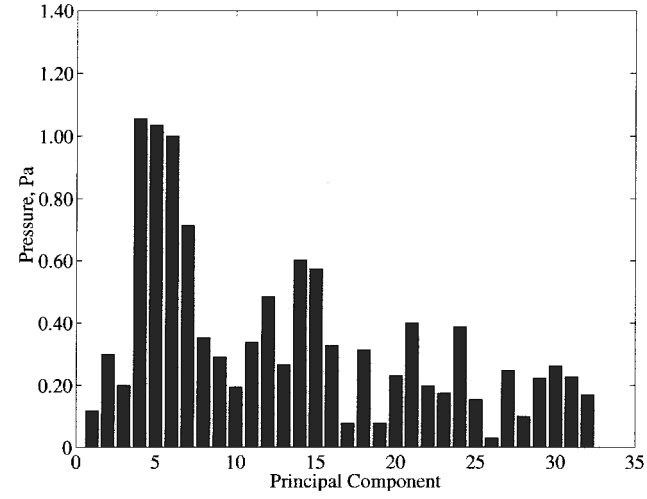

Fig. 11 Primary PCs, second harmonic.

as much of the primary source in the first 18 principal components as possible. The principal component distribution of the first harmonic (BPF) is well constructed (Fig. 10) with most of the acoustic power in the lower PCs. The second harmonic (2BPF) PC distribution is good (Fig. 11), whereas the third harmonic PC distribution is only fair (Fig. 12) with acoustic power building in the higher, least efficient PCs.

Noise Control Results

The results of the noise control flight test are discussed here, including coherence data between the synchrophaser and the interior sound field and noise reductions obtained at the first three harmonics of the propeller BPF. The section begins with a description of the test procedure used during the flight.

Test Procedure

The flight began with a climb to a cruising altitude of 15,000 ft, at which point the pilot reduced the engine speed from the cruise engine speed from 1550 to 1440 rpm. This shifted the propeller BPF and its harmonics away from their cruise operating frequencies, thereby allowing the control system to measure the transfer functions between actuators and error sensors at the 1550-rpm operating frequencies. The transfer functions were measured in flight by exciting an individual actuator with one of the first three harmonics of the normal BPF while recording the microphone responses.

Once the system identification was completed, the pilot restored the engines to their cruise operating speed, and the noise reduction

Table 5 Test points

Run no.	Activity	Time, min
	System identification	28
1a	Control BPF	7
1b	Control 1,2,3 BPF linear	6
3a	Control 1,2,3 BPF A weighted	6
5a	Control 1,2,3 BPF linear	7
6a	Control 2 BPF	4
7a	Control 1,2,3 BPF, descent	17

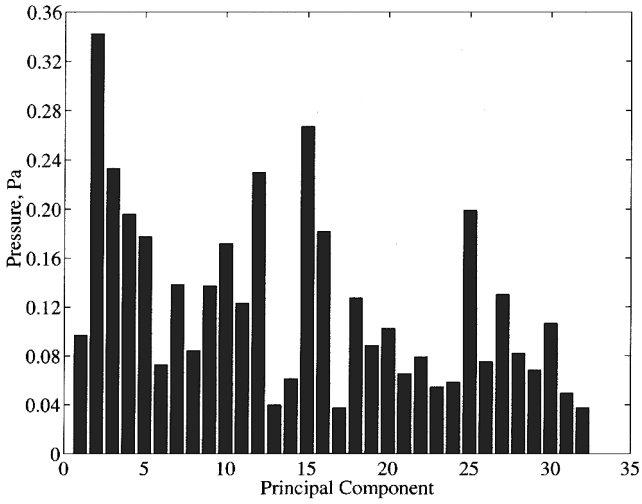

Fig. 12 Primary PCs, third harmonic.

tests were started. The test points obtained during the flight are listed in Table 5. The first column in Table 5 gives the run number for the test points; these numbers will be used subsequently when the results are discussed. The next two columns contain a description of each test point and the approximate length in minutes of each test. The notation BPF and 2BPF denote the blade passage frequency and its second harmonic, respectively. All of the test points listed in Table 5 were conducted with the control system synchronized to the left (portside) engine. The total elapsed time from the start of the system identification procedure to touchdown was 79 min.

Operational Strategy

The step size parameter μ and control effort penalty β must be set for each virtual PC channel. For the multifrequency PC-LMS controller this totals 108 parameters (3 frequencies times 18 PCs per frequency times 2 parameters per PC). The appropriate values for these parameters were not known ahead of time, and so the system was initialized with a small step size and an effort penalty large enough to prohibit any control output. The effort penalties for a particular frequency PC were then relaxed incrementally and the control system response observed from a monitoring station that displayed the average noise power at the microphones and the total control voltages. For multifrequency tests, the test engineer relied on a performance metric (Δ decibels per watt) that was calculated and displayed for each frequency to decide where additional control effort should be applied to produce the most noise reduction. This resulted in long apparent convergence times, which were acceptable given that a primary goal of the control system for these tests was predictable and stable operation. If predictable and stable operation is achieved (as it was in this flight test) then it is possible to implement an outer loop controller, for example, in fuzzy logic, that would automatically adjust the inner loop parameters, reducing convergence times dramatically.

Coherence Results

The coherence between the reference signal and the primary noise field determines the maximum possible noise reduction in a feedforward control system.[12] The reference signal was generated on the DSP synchronously with the tachometer signal taken from the port engine. One would, therefore, expect relatively good coherence between the reference and the noise field created by the portside propeller. Because the interior noise field contains contributions from the port and starboard propellers, the coherence may be reduced, dependent on the precision of the aircraft's synchrophaser. Another factor contributing to reduced coherence may be a lack of coherence between the engine tachometer signal and the interior noise field due to uncorrelated effects such as aerodynamic buffeting.

Figure 13 shows the coherence between the reference and the microphone responses, as measured during test 5a (see Table 5). The x axis denotes the microphone channel ranging from 1 to 32, except for channel 7, which was inoperable during the tests and, therefore, is not plotted. The coherence is shown at the first three harmonics of the blade passage frequency, BPF, 2BPF, and 3BPF. The coherence values are generally high and show a slight drop off with increasing harmonic number. One would expect to see greater microphone-to-microphone variation at the higher frequencies where the wavelengths are shorter.

First Harmonic (BPF) Results

The first test concerned the reduction of the propeller BPF. The uncontrolled sound pressure level (SPL) averaged across the microphone array is shown in Fig. 14. The harmonics of the BPF are evident at 103, 206, 309, and 412 Hz. The tone at 160 Hz was associated with the environmental control system on the aircraft and was not targeted by the noise reduction system during these tests. A time history of the average SPL of the BPF after the control system was turned on is shown in Fig. 15. The solid line shows the measured SPL at approximately 1-s intervals during the 6.75-min test.

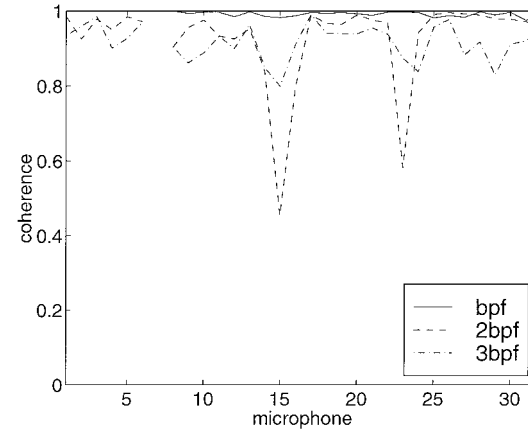

Fig. 13 Reference to primary coherence, run 5a.

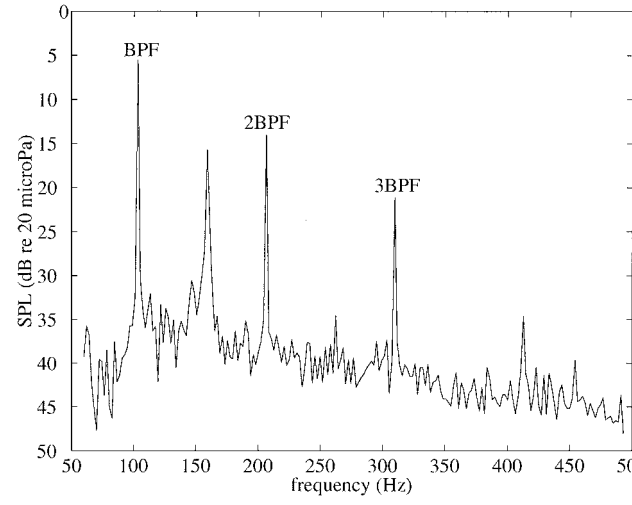

Fig. 14 Average SPL before control, run 1a.

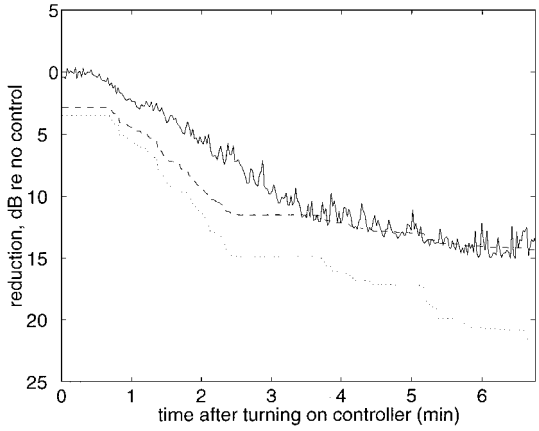

Fig. 15 Reduction of BPF: ——, measured; - - - -, predicted; and . . . . . , predicted using unity coherence.

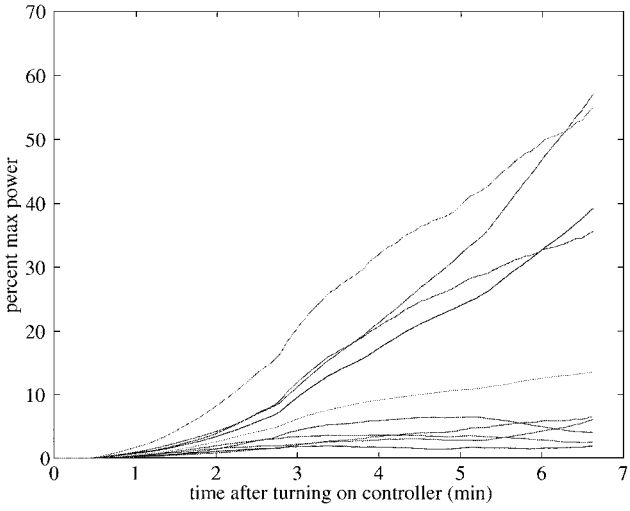

Fig. 16 Actuator maximum power.

The other lines show the predicted noise reduction; the dashed line includes effort constraints and measured coherence, and the dotted line includes effort constraints but assumes unity coherence. The effort constraints were reduced incrementally during the test, hence the stair-step appearance of the predicted noise reduction. The SPL of the BPF was reduced by nearly 15 dB 6 min after the control system was turned on. The measured reduction closely matches the predicted value (dashed line), which illustrates the importance of coherence in noise reduction prediction.

Actuator Power

A primary concern in the design of the noise control system was to ensure that the actuators had sufficient authority. Figure 16 is a plot of the percent of actuator maximum power consumed during this test for 10 of the most utilized actuators. At the end of the test, a few actuators approached 60% power (about 7 W), well below the 12-W maximum. By the use of Fig. 15 in conjunction with Fig. 16, it is possible to trade off actuator power for noise reduction, thereby selecting a noise reduction figure that would require a less powerful, but cheaper, actuator. Also notice that, even though noise reduction is leveling off, actuator power is climbing steadily, thus emphasizing the need for force constraints.

Multifrequency Results

Two multifrequency tests were conducted in which the first three harmonics were controlled simultaneously. The goal of the first test (run 1b in Table 5) was to minimize a linear summation of the levels of the three harmonics, as given by Eq. (14). From the uncontrolled harmonic levels shown in Fig. 14, this amounted to reducing the BPF first, then the second harmonic, and then applying any remaining control authority to the third harmonic. The goal of the second test (run 3a in Table 5) was to minimize an A-weighted summation of the harmonic levels. This amounted to reducing the third harmonic, followed by the second, and then the BPF itself. The end result of these two tests was similar; small reductions were obtained at the two higher harmonics because most of the control energy was spent where it was most effective, namely, on the BPF.

Linear Cost Function

Time histories showing the reduction in a linear and an A-weighted summation of the three harmonics are plotted in Fig. 17. The linear cost was reduced by slightly more than 8 dB (4 dBA) during the test . The test was approximately 6 min long and produced noise reductions at the first three harmonics of 9.5, 3.3, and 1.5 dB, respectively.

A-Weighted Cost Function

Measured reductions in the first three harmonics of 10, 2.5, and 3.0 dB, respectively, were obtained. Compared to the results from test 1b, there was an improvement at the third harmonic, from 1.5 to 3.0 dB of reduction, but this came at the expense of the second harmonic, which was reduced by only 2.5 dB in this test.

A time history of the cost function reduction is plotted in Fig. 18. The A-weighted reduction of the three harmonics was just over 4 dB, which is nearly identical to the reduction that was obtained in test 1b. The linear reductions were also nearly equal between the two tests.

The actual multifrequency noise reductions are listed in Table 6. The first harmonic performs close to predictions (see Table 4),

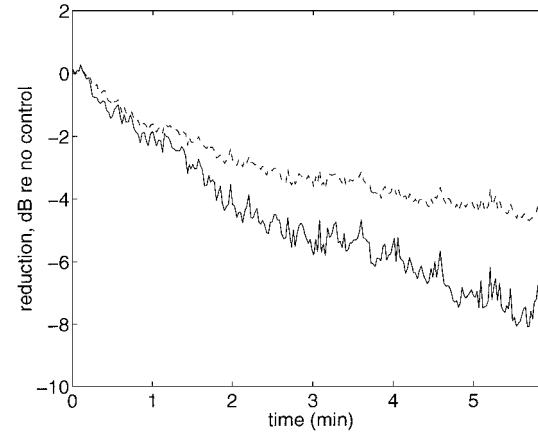

Fig. 17 Reduction of cost function (run 1b, linear-weighted cost): ——, linear, and - - - -, A weighted.

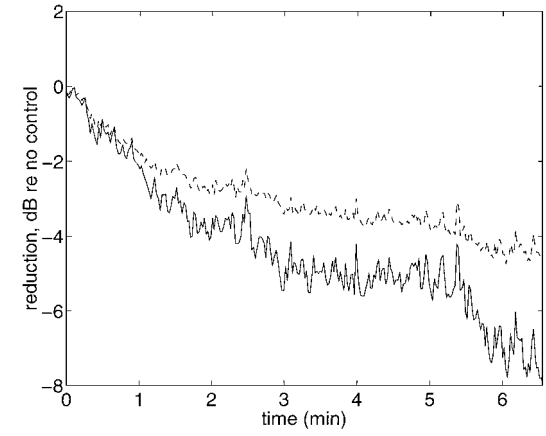

Fig. 18 Reduction of cost function (run 3a, A-weighted cost): ——, linear, and - - - -, A weighted.

Table 6 Multifrequency noise control attained for runs 1b (linear) and 3a (A weighted)

	ΔdB			
Weighting	Overall	BPF	2BPF	3BPF
Linear	−8	−9.5	−3.3	−1.5
A weighted	−4	−10.0	−2.5	−3.0

whereas the second and third harmonics performance falls well below. The similarity of this behavior to that in Table 3 indicates that cabin pressurization may have affected the optimization results.

Concluding Remarks

The active structural/acoustic control system attained good control of the blade passage frequency in single-frequency (15-dB) and multifrequency (10-dB) tests. Control of the second and third harmonics did not meet expectations (expected ~7, obtained ~3 dB). This was due possibly to the effect of cabin pressurization on the structural/acoustic transfer functions. The transfer functions were obtained in unpressurized conditions on the ground and used for actuator location optimization. The resulting actuator array was probably suboptimally placed, an effect having a greater impact at the higher harmonics. When in-flight transfer functions are used, predictive capability is shown to be excellent. The use of the actuator array optimization technique can then be recommended if good transfer functions are available. The principal component control system proved to be highly configurable and remained stable throughout the test matrix. The ASAC approach has been shown to be very efficient, requiring a maximum of 7 W of power per actuator to produce 15-dB noise reduction in the first harmonic.

References

[1]Fuller, C. R., and Jones, J. D., "Experiments on Reduction of Propeller Induced Interior Noise by Active Control of Cylinder Vibration," *Journal of Sound and Vibration*, Vol. 112, No. 2, 1987, pp. 389–395.

[2]Lester, H. C., and Lefebvre, S., "Piezoelectric Actuator Models for Active Sound and Vibration Control of Cylinders," *Journal of Intelligent Material Systems and Structures*, Vol. 4, July 1993, pp. 295–306.

[3]Snyder, S. D., and Hansen, C. H., "Mechanisms of Active Noise Control by Vibration Sources," *Journal of Sound and Vibration*, Vol. 147, No. 3, 1991, pp. 519–525.

[4]Silcox, R. J., Lefebvre, S., Metcalf, V. L., Beyer, T. B., and Fuller, C. R., "Evaluation of Piezoceramic Actuators for Control of Aircraft Interior Noise," AIAA Paper 92-02-091, May 1992.

[5]Thomas, D. R., Nelson, P. A., and Elliott, S. J., "Active Control of the Transmission of Sound Through a Thin Cylindrical Shell, Part II: The Minimization of Acoustic Potential Energy," *Journal of Sound and Vibration*, Vol. 167, No. 1, 1993, pp. 113–128.

[6]Elliott, S. J., Nelson, P. A., Stothers, I. M., and Boucher, C. C., "In-Flight Experiments on the Active Control of Propeller-Induced Cabin Noise," *Journal of Sound and Vibration*, Vol. 140, No. 2, 1990, pp. 219–238.

[7]Dorling, C. M., Eatwell, G. P., Hutchins, S. M., Ross, C. F., and Sutcliffe, S. G. C., "A Demonstration of Active Noise Reduction in an Aircraft Cabin," *Journal of Sound and Vibration*, Vol. 128, No. 2, 1989, pp. 358–360.

[8]Ross, C. F., and Purver, M. R. J., "Active Cabin Noise Control," *Proceedings of the International Symposium on Active Control*, European Acoustics Association, Paris, 1997, pp. 39–46.

[9]Elliott, S. J., Stothers, I. M., and Nelson, P. A., "A Multiple Error LMS Algorithm and Its Application to the Active Control of Sound and Vibration," *IEEE Transactions on Acoustics, Speech, and Signal Processing*, Vol. ASSP-35, No. 10, 1987, pp. 1423–1434.

[10]Cabell, R.H., "A Principal Component Algorithm for Feedforward Active Noise and Vibration Control," Ph.D. Dissertation, Dept. of Mechanical Engineering, Virginia Polytechnic Inst. and State Univ., Blacksburg, VA, May 1998.

[11]Palumbo, D. L., and Padula, S. L., "Optimization of an Actuator Array for the Control of Multifrequency Noise in Aircraft Interiors," AIAA Paper 97-1615, May 1997.

[12]Nelson, P. A. and Elliott, S. J., *Active Control of Sound*, Academic, New York, 1992, pp. 379–410.

[13]Caton, J. L., *An Investigation Into the Control Robustness of Active Structural Acoustic Control in Aircraft Cabin Models.* M.S. Thesis, School of Engineering and Applied Science, George Washington Univ., Newport News, VA, Aug. 1998.

[14]Palumbo, D. L., and Cabell, R. H., "Optimizing Sensor and Actuator Arrays for ASAC Noise Control," Society of Automotive Engineers Paper 2000-01-1707, May 2000.

[15]Rossetti, D. J., Jolly, M. R., and Southward, S. C., "Control Effort Weighting in Feedforward Adaptive Control Systems," *Journal of the Acoustical Society of America*, Vol. 99, No. 5, 1996, pp. 2955–2964.